IEEE Access
Multidisciplinary ⋮ Rapid Review ⋮ Open Access Journal

Received 20 March 2023, accepted 10 April 2023, date of publication 14 April 2023, date of current version 25 April 2023.

Digital Object Identifier 10.1109/ACCESS.2023.3267159

RESEARCH ARTICLE

Cogging Torque Suppression of Modular Permanent Magnet Machines Using a Semi-Analytical Approach and Artificial Intelligence

ELIA BRESCIA[1], MARCO PALMIERI[2], (Member, IEEE), PAOLO R. MASSENIO[1], GIUSEPPE L. CASCELLA[1], (Member, IEEE), AND FRANCESCO CUPERTINO[1], (Senior Member, IEEE)

[1]Department of Electrical and Information Engineering, Polytechnic University of Bari, 70125 Bari, Italy
[2]School of Engineering, Università degli Studi della Basilicata, 85100 Potenza, Italy

Corresponding author: Elia Brescia (elia.brescia@poliba.it)

This work was supported in part by the Project InSITE–INtelligent Energy Management of Smartgrids Based on IoT and Edge/Cloud Technologies–Bando di gara per progetti di ricerca di cui all'art. 10, comma 2, lettera (b) del decreto 26 gennaio 2000, previsti dal Piano triennale 2019–2021 della Ricerca di sistema elettrico nazionale–Program under Grant CSEAB_00320; and in part by the Project NextGenerationEU (Partenariato Esteso Scenari Energetici del Futuro–NEST) under Grant CUP D93C22000900001.

ABSTRACT The cogging torque of permanent magnet machines with a modular stator is affected by additional harmonic components due to the segmentation of the stator lamination. This paper proposes a novel approach based on the shaping of the stator tooth tips with sinusoidal profiles to minimize the cogging torque of such machines. A theoretical study and a design formula are proposed to determine the spatial frequency of the sinusoidal profiles, while an optimization procedure based on genetic algorithm and artificial neural networks is adopted to determine their amplitudes and phase shifts. The proposed method is validated through finite element analysis considering two different case studies. Also, a comparison with other approaches from the literature is presented to highlight the effectiveness of the proposed technique. Finally, an additional analysis is reported to demonstrate the effectiveness of the proposed method against manufacturing and assembling tolerances.

INDEX TERMS Artificial neural networks, cogging torque, finite-element analysis, genetic algorithm, modular stators, permanent magnet synchronous motors, segmented stators, surrogate modeling.

I. INTRODUCTION

Permanent magnet machines (PMMs) with a modular, i.e. segmented, stator core are gaining increasing interest. In the last years, different studies have highlighted many advantages of such machines if compared to conventional PMMs with a one-piece stator. In fact, a modular stator core allows to enhance the slot fill factor, to ease the manufacturing process and coil winding and to reduce the end winding and iron wastage [1], [2], [3]. These advantages are noticeable both in large machines, such as wind and tidal generators [4], [5], as well as in low power and small size PMMs [6], [7], [8]. Also, many works studied the features of PMMs with a segmented stator core. For instance, [2], [7], and [9], show how the additional stator gaps between the stator modules influence the electromagnetic performances. The influence of the stator segmentation on mechanical vibrations and acoustic noise is analyzed in [3], while [10] proves the resistance capabilities of modular surface mounted PMMs against irreversible demagnetizations.

However, the additional stator gaps in the flux path of modular stator PMMs generate additional harmonic components

The associate editor coordinating the review of this manuscript and approving it for publication was Wei Wei.

This work is licensed under a Creative Commons Attribution 4.0 License. For more information, see https://creativecommons.org/licenses/by/4.0/

(AHCs) of the cogging torque [11]. That is, an undesired torque pulsation also at no-load condition, which increases vibrations, acoustic noise and speed pulsations. Compared to the native harmonic components (NHCs) of the cogging torque in conventional PMMs with a one-piece slotted stator, the AHCs have lower harmonic orders and higher amplitudes [11], [12].

The minimization of the NHCs of the cogging torque in one-piece stator PMMs has been addressed using rotor or stator skewing [13], [14], dummy slots or notches on the tooth tips [15], [16], slot openings design [17], [18] and teeth pairing [19], [20]. Both analytical and meta-heuristic approaches are adopted to determine the optimal design solutions. For instance, in [21], an analytical approach using conformal mapping method is employed to determine the optimal shifting angle of the slot openings to minimize the cogging torque. In [22], the optimum arrangement of PMs to reduce cogging torque is found by means of analytical studies in which the PMs magnetization is described using the Fourier series and the effect of the slots on the airgap flux density is taken into account with the equivalent magnetizing current method. In [23], a genetic algorithm coupled with finite-element analysis (FEA) is proposed to determine the position of PMs which minimizes the cogging torque. In [23], the cogging torque of a brushless DC motor is minimized using a genetic algorithm and Kriging surrogate models.

However, such methods cannot be applied for the minimization of the AHCs in modular stator PMMs. In fact, the rotor skewing has no influence on low order AHCs [25], while the design of a unique shape for all the stator tooth tips has a limited effectiveness in AHCs minimization as shown in [26] and [27]. Thus, placing equally spaced dummy slots in the stator is ineffective as well.

The explicit minimization of the cogging torque of PMMs with modular stators has received poor attention from the research community. In [11], an optimal number of uniform stator modules or an optimal combination of non-uniform stator modules are proposed. However, although strict limitations are imposed in the machine design phase, the results showed a non-negligible residual cogging torque. In [4], the stator slot openings shifting is proposed to mitigate the cogging torque of a modular stator PMM with E-shaped stator modules. Nevertheless, the effectiveness of such method fails in case of some specific topologies due to the limited impact of the slot openings on the cogging torque. In [26] and [27], a method based on the design of multiple shapes of the tooth tips with a topological optimization is presented. The optimal geometry of the tooth tips is found by means of a genetic algorithm (GA) and a finite element analysis (FEA) in [26] or surrogate models trained with FEA results in [27]. Compared to [4], this approach handles arbitrary topologies with uniform stator segments. However, this method requires a complex design procedure to discretize the tooth tips in the finite element model. Moreover, the number of design variables depends on the number of stator modules, stator slots, machine poles and on the number of binary elements in which each tooth tip is discretized. Therefore, the computational efforts required by [26] and [27] significantly increase in case of specific topologies where the number of design variables is very high.

This paper proposes an alternative design method aimed at minimizing the AHCs of the cogging torque of modular PMMs. This method uses sinusoidal profiles to shape the tooth tips, which is an approach mainly used to contour the permanent magnets in order to increase the generated torque while reducing the NHCs of the cogging term in one-piece stator superficial PMMs (SPMMs) [28], [29]. As in [26] and [27], the proposed method handles arbitrary topologies with uniform stator segments. However, compared to the topological optimization in [26] and [27], the design procedure is simplified. In fact, sinusoidal profiles are easily reproducible in the finite element model and their number depends only on the number of AHCs to minimize, ensuring a computationally-efficient approach. A theoretical study supports the choice of the spatial frequency of the sinusoidal profiles, while an optimization procedure is set up to find their amplitudes and positions.

The main contributions and features of this work are as follows:

1) A novel method to reduce the cogging torque of modular PMMs is proposed.
2) Compared to [4], this method has a wider range of application since it handles different modular topologies.
3) Compared to [11], this method does not impose limitations in the machine design phase.
4) Compared to [26] and [27], this method offers a more simple and computational-efficient solution.

II. COGGING TORQUE OF PMMs WITH MODULAR STATOR CORES

The cogging torque of slotted PMMs with modular stators can be expressed as in [11] by:

$$T_{cog}(\vartheta_r) = T_{NHC}(\vartheta_r) + T_{AHC}(\vartheta_r), \tag{1}$$

where ϑ_r is the rotor angular position, T_{NHC} expresses the NHCs caused by the stator slots and T_{AHC} expresses the AHCs caused by the modular stator core.

The angular frequency of the NHCs is an integer multiple of the least common multiple (LCM) between the number of stator slots N_s and the number of poles $2p$, while the frequency of the AHCs is an integer multiple of the LCM between $2p$ and the number of stator core modules m. Thus, it results that:

$$T_{NHC} = \sum_i^{\infty} T_{NHCi} \sin(\mathrm{LCM}(2p, N_s)\, i\vartheta_r + \varphi_{NHCi}), \tag{2}$$

$$T_{AHC} = \sum_i^{\infty} T_{AHCi} \sin(\mathrm{LCM}(2p, m)\, i\vartheta_r + \varphi_{AHCi}), \tag{3}$$

where T_{NHCi}, T_{AHCi}, φ_{NHCi} and φ_{AHCi} are the amplitudes and the phase shifts of the i-th harmonic components.

Since the number of stator slots is an integer multiple of the number of stator core modules, then LCM $(2p, m) \leq$ LCM $(2p, N_s)$ and the harmonic orders of the AHCs can be lower than those of the NHCs. Moreover, once the number of poles is fixed, the amplitudes of the AHCs increase when LCM $(2p, m)$ decreases [11].

III. TOOTH TIPS HARMONIC SHAPING

This section describes the method to minimize the cogging torque based on the harmonic shaping of the tooth tips. Subsection III-A presents an analytical study aimed at determining the number and the spatial frequency of the sinusoidal profiles required to suppress the cogging torque harmonics. Subsection III-B deals with determining the optimal amplitudes and phase shifts of the introduced sinusoidal profiles. Finally, Subsection III-C describes the proposed approach to solve the optimization problem formulated in the previous section.

A. THEORETICAL STUDY AND DESIGN FORMULA

Following the approach proposed in [27], the present study investigates the introduction of additional harmonics in the airgap permeance function to suppress the AHCs caused by the modular stator core. The cogging torque of a PMM featuring tooth tips with a modified shape can be expressed as:

$$T_{cog}(\vartheta_r) = T_{NHC}(\vartheta_r) + T_{AHC}(\vartheta_r) + T_{IHC}(\vartheta_r), \quad (4)$$

where T_{IHC} are the cogging torque harmonics introduced by the modified shapes of tooth tips, namely the introduced harmonic components (IHC). In [27], the IHCs are investigated considering the coenergy method and the superposition principle. The latter allows to study the IHCs considering a non-modular stator core, i.e., these torque harmonics can be expressed as:

$$T_{IHC}(\vartheta_r) = -k_g \frac{\partial}{\partial \vartheta_r} \int_0^{2\pi} \Lambda'_{tts}(\alpha) F_m^2(\alpha, \vartheta_r)\, d\alpha, \quad (5)$$

where k_g is a constant which depends on the geometrical parameters of the PMM, Λ'_{tts} is a component of the squared airgap permeance function introduced by the modified shapes of the tooth tips and F_m is the rotor magneto-motive force (MMF); α is the angular displacement along the stator circumference. In [27] the authors proved how the frequencies of the harmonic components of $\Lambda'_{tts}(\alpha)$ are equal to the spatial frequencies of the harmonic components of the function expressing the additional airgap flux-path length due to the modified shape of the tooth tips. In this case, the additional airgap flux-path length depends on the sinusoidal profiles shaping the tooth tips. Therefore, it can be stated that a unique harmonic of Λ'_{tts} is introduced for each sinusoidal profile and that these share the same spatial frequencies.

Considering (5), for the orthogonality of the trigonometric functions, only the isofrequential harmonic components of $\Lambda'_{tts}(\alpha)$ and $F_m^2(\alpha, \vartheta_r)$ contribute to the cogging torque. Let N_{sp} be the number of introduced sinusoidal profiles and f_{IHC_k} be the spatial frequency, expressed in rad^{-1}, of the k-th sinusoidal profile introduced to shape the tooth tips. Hence, the Fourier series of the IHCs produced by N_{sp} sinusoidal profiles used to shape the tooth tips is as follows

$$T_{IHC}(\vartheta_r) = \sum_{k=1}^{N_{sp}} T_{IHC_k} \sin\left(2\pi f_{IHC_k} \vartheta_r + \varphi_{IHC_k}\right), \quad (6)$$

where T_{IHC_k} and φ_{IHC_k} are the amplitude and the phase shift of the k-th harmonic component, respectively.

To suppress the AHCs, the IHCs should have the same frequencies. Let now $N_{AHC} \subset \mathbb{N}$ be the set of the harmonic orders of the AHCs to minimize. Considering (3) and (6), the following relations must be satisfied

$$2\pi f_{IHC_k} = \text{LCM}(2p, m)\, i, \quad (7)$$

$$f_{IHC_k} = \frac{\text{LCM}(2p, m)\, i}{2\pi},\ i \epsilon N_{AHC}. \quad (8)$$

Equation (8) represents the design formula which allows to choose the frequency of the sinusoidal profiles employed to shape the tooth tips of the PMM with a modular stator core.

Note that the same methodology can be also applied to reduce the NHCs. Let be $N_{NHC} \subset \mathbb{N}$ the set of the NHCs to minimize. According to (2) and (6), the IHCs required to suppress the NHCs should have the following frequencies

$$f_{IHC_k} = \frac{\text{LCM}(2p, N_s)\, j}{2\pi},\ j \epsilon N_{NHC}. \quad (9)$$

Note how (9) can be also employed for the suppression of the cogging torque of conventional PMMs with a one-piece stator core. Note also that from (8) and (9), a sinusoidal profile should be introduced for each cogging torque harmonic component to be suppressed. Therefore, N_{sp} is equal to the number of harmonic components of the cogging torque to be minimized.

B. FORMULATION OF THE OPTIMIZATION PROBLEM

Equations (8) and (9) allow the designer to choose the number and frequency of the sinusoidal profiles which introduce cogging torque harmonic components with the same frequencies of the AHCs and NHCs to be minimized. However, to suppress both the AHCs and NHCs, it is also necessary to properly set the amplitude and position of the sinusoidal profiles. Fig. 1 shows a linearized representation of two tooth tips shaped through the composition of two sinusoidal profiles, where:

$$r(\alpha) = S(\alpha, \boldsymbol{A}, \boldsymbol{\varphi}) + |\min(S(\alpha, \boldsymbol{A}, \varphi))|, \quad (10)$$

$$S(\alpha, \boldsymbol{A}, \boldsymbol{\varphi}) = \sum_{k=1}^{N_{sp}} A_k \cos\left(2\pi f_{IHC_k} \alpha + \varphi_k\right), \quad (11)$$

$$\boldsymbol{A} = [A_1 A_2 \ldots A_{N_{sp}}], \quad (12)$$

$$\boldsymbol{\varphi} = \left[\varphi_1 \varphi_2 \ldots \varphi_{N_{sp}}\right], \quad (13)$$

in which A_k and φ_k are the amplitude (mm) and phase shift of the introduced sinusoidal profiles, respectively. To determine the optimal amplitudes and phase shifts of the introduced

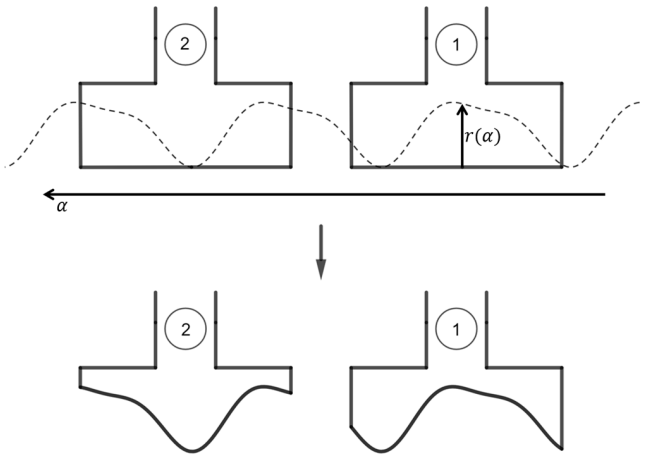

FIGURE 1. Tooth tips shaped with two combined sinusoidal profiles.

sinusoidal profiles, the following optimization problem is defined:

$$\min f(\boldsymbol{x}) \tag{14}$$

with

$$f(\boldsymbol{x}) = \max\left(T_{cog}(\boldsymbol{x}, \vartheta_r)\right) - \min\left(T_{cog}(\boldsymbol{x}, \vartheta_r)\right),$$
$$\boldsymbol{x} = [\boldsymbol{A}\boldsymbol{\varphi}], A_i \epsilon [0\, A_{lim}], \varphi_i \epsilon [0\, 2\pi], i = 1, \ldots, N_{sp} \tag{15}$$

in which $\boldsymbol{x}$ is the vector of the design variables and A_{lim} is the upper bound for the amplitude of the sinsuodial profiles. Moreover, the following constraint is introduced:

$$S(\alpha, \boldsymbol{A}, \varphi) \leq A_{lim}. \tag{16}$$

The manufacturing feasibility of the tooth tips is ensured by setting A_{lim} less or equal to half of the tooth tips height.

C. HEURISTIC OPTIMIZATION USING GA AND ANN-BASED SURROGATE MODELS

The optimization problem in the previous section is solved using a GA which employs ANN-based surrogate models to compute the objective function in (14). In fact, an analytical approach to compute the cogging torque of the PMM, even though computationally fast, would result poorly accurate and difficult to set-up due to the complex geometries of the machines and to the non-linearities of the magnetic materials. FEA is commonly employed to overcome the limitations of analytical models [30] and meta-heuristic algorithms are adopted to solve this class of optimization problems [23], [23], [31]. However, this approach requires a huge computational burden due to the number of iterations needed by the meta-heuristic algorithms to find an acceptable solution. Therefore, the use of surrogate-models trained by a small amount of FEA simulations chosen with a proper design of experiment (DoE) can result an effective alternative since it guarantees a good accuracy while mitigating, at the same time, the computational effort required by the evaluation and minimization of the objective function [32], [33].

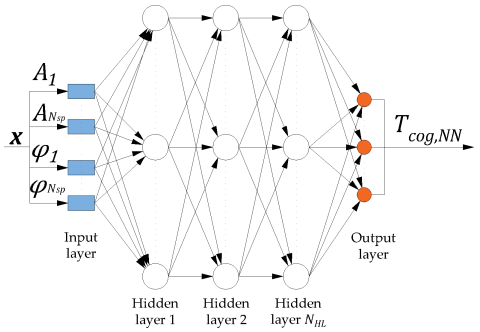

FIGURE 2. Architecture of the proposed ANN-based surrogate model.

The optimization procedure proposed in this paper is divided into three main stages:

1) DOE

An arbitrary number (N_{DOE}) of solutions ($\boldsymbol{x}$) uniformly and randomly sampled in a discrete subspace (X) of the design space defined by (15) is obtained. The corresponding cogging torque ($f(\boldsymbol{x})$) is computed by means of a transient-with-motion (TWM) FEA using the Simcenter MagNet software. The TWM FEA accurately computes the torque of the modular PMM considering a predefined number of rotor positions (N_{pos}) within a two-poles pitch. A particular attention is posed on setting this quantity, as N_{pos} affects both the computational burden of the TWM FEA and the accuracy of the torque analysis. In agreement with the Shannon's sampling theorem, the number of rotor positions analyzed by the TWM FEA should be at least twice the highest cogging torque harmonic component to be minimized (i_{max}); in this paper, it is set $N_{pos} = 6i_{max}$. The output of the TWM FEA is a vector ($\boldsymbol{T_{cog,FEA}}(\boldsymbol{x}, \vartheta_r)$) of N_{pos} values of the cogging torque.

2) SURROGATE MODELS DESIGN AND TRAINING

A multi-layer feed-forward (FF) ANN, with the structure depicted in Fig. 2 is chosen as surrogate model. This FF ANN consists of N_{HL} hidden layers with N_{HN} neurons per layer, where each neuron features a hyperbolic tangent sigmoid as activating function. The input layer is the vector of the design variables $\boldsymbol{x}$. The output layer consists of N_{pos} linear neurons whose output is $\boldsymbol{T_{cog,NN}}(\boldsymbol{x}, \vartheta_r)$, i.e. the vector containing the N_{pos} values of the cogging torque over a two-poles pitch angle. ANNs adopted as surrogate models for optimization purposes ensure high approximation performances with low computation burden [34]. However, to optimize the accuracy and the computational cost of an ANN, a careful design of its topology is required, in particular with respect to the number of neurons per layer and the number of hidden layers [35]. In this paper, to choose the optimal topology of the ANN-based surrogate models, the following procedure is developed:

- Step 1: random splitting of the dataset obtained with the DoE in training data (80%), validation data (15%), and test data (5%).

- Step 2: training instances of the ANNs with all the possible topologies with $N_{HL} \in \mathbb{N}_{HL}$ and $N_{HN} \in \mathbb{N}_{HN}$, where $\mathbb{N}_{HL}$ and $\mathbb{N}_{HN}$ are the set of the allowed values of the number of hidden layers and number of neurons per layer, respectively. To avoid the overfitting of the ANN, a training stop criterion based on the maximum validation failures is considered. The training of an ANN is stopped if the estimation error on the validation data fails to improve for ten epochs in a row. At the end of the training, the estimation error on the test data is stored.
- Step 3: steps 1 and 2 are repeated N_{tr} times.
- Step 4: the ANN topology with the lowest average estimation error on the test data is chosen as surrogate model.
- Step 5: final training of the chosen surrogate model with a random splitting of the dataset in training data (80%) and validation data (20%). In this case, the training of the surrogate model is stopped if the estimation error on the validation data fails to improve for ten epochs in a row.

3) GA OPTIMIZATION AND FEA VALIDATION

A GA is finally implemented to solve the optimization problem (14)-(16) considering the following surrogate objective function:

$$\min f_{NN}(\boldsymbol{x}) \text{ with}$$
$$f_{NN}(\boldsymbol{x}) = \max\left(\boldsymbol{T}_{\boldsymbol{cog,NN}}(\boldsymbol{x})\right) - \min\left(\boldsymbol{T}_{\boldsymbol{cog,NN}}(\boldsymbol{x})\right). \quad (17)$$

This objective function expresses the optimization problem (14) considering the use of the surrogate model to compute the cogging torque of the modular PMM. The GA is a stochastic evolutionary algorithm that modifies a population of individual solutions according to rules that mimic biological evolution. At each iteration, the GA selects individuals from the current population to be parents producing the individuals for the next generation.

A drawback of the GA is that it can easily converge to suboptimal solutions if the number of individuals and generations is not carefully chosen [36], [37]. The main limitation to the use of high numbers of individuals and generations is the computational effort required for the objective function computation. However, due to the to the high computational efficiency of the surrogate models, a GA with a high number of individuals and generations can be used to perform the optimization (17) thus reducing the risk to converge to suboptimal solutions.

Due to the approximation error of the surrogate models, a validation using a TWM FEA is performed to rigorously evaluate the solution $\boldsymbol{x}$ found by the GA. Therefore, the objective function (18) is finally evaluated using a TWM FEA:

$$f_{FEA}(\boldsymbol{x}) = \max\left(\boldsymbol{T}_{\boldsymbol{cog,FEA}}(\boldsymbol{x}, \vartheta_r)\right) - \min\left(\boldsymbol{T}_{\boldsymbol{cog,FEA}}(\boldsymbol{x}, \vartheta_r)\right). \quad (18)$$

TABLE 1. Main parameters of the APMG.

Symbol	Parameter	Value
-	rated torque	19 Nm
-	rated speed	941 rpm
-	rated current	1.55 A
m	number of modules	20, 60
p	number of pole pairs	50
N_s	number of slots	120
-	Stator back-iron thickness	3.3 mm
-	Rotor back-iron thickness	4.5 mm
-	PM thickness	3.5 mm
-	Axial length	10 mm
-	Air gap length	6.5 mm
-	Stator external radius	583 mm
-	Tooth tip width	21 mm
-	Tooth tips height	2 mm
-	Tooth width	3.9 mm
-	Stator external radius	583 mm

TABLE 2. Main optimization parameters.

Parameter	Value
A_{lim}	0.75 mm
$\mathbb{N}_{HL}$	[2 4 6 8 10 12 14 16 18 20]
$\mathbb{N}_{HN}$	[1 2 3]
N_{tr}	20
GA population size	400
GA maximum generations number	400
GA crossover/mutation rate	80% / 20%
GA number of elite individuals	0.05·Population size

IV. RESULTS

The proposed method is validated on two different topologies of a modular annular PM generator (APMG) designed for a low power ducted wind turbine. This generator has a large diameter and a small axial length which justifies the adoption of a modular structure to simplify the manufacturing and assembling process. The main design aspects of the APMG can be found in [38], while its parameters are summarized in TABLE 1. Instead, the values of the parameters required by the proposed optimization procedure are reported in TABLE 2.

The results obtained with sinusoidal profiles designed in agreement with the design formula (8) are reported in Subsection IV-A, while Subsection IV-B reports the results obtained with sinusoidal profiles designed in disagreement with the design formula. Subsection IV-C shows the cogging torque obtained with the methods proposed in [4] and [27] and Subsection IV-D reports a detailed comparison of the optimized and basic designs of the APMG at rated current. Finally, Subsection IV-E analyzes the influence of manufacturing and assembling tolerances on the performance of the proposed method.

A. RESULTS USING THE DESIGN FORMULA

Fig.3 shows the basic design of the APMGs with 20 and 60 stator core modules. According to (3), for these two topologies, the following harmonic orders of the AHCs are expected

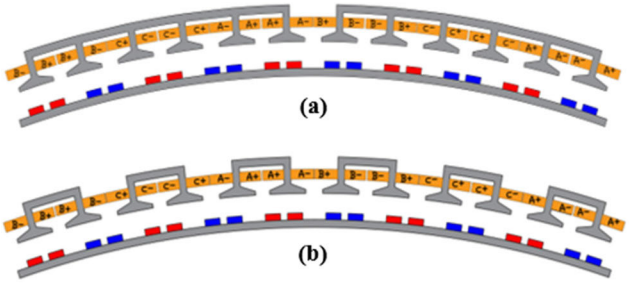

FIGURE 3. Portion of the APMG with 20 stator core modules (a), portion of the APMG with 60 stator core modules (b).

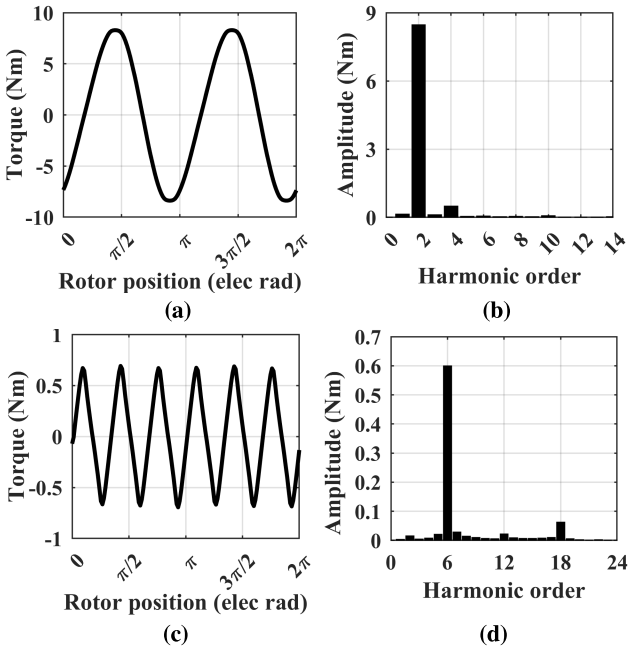

FIGURE 4. Cogging torque profile (a) and harmonic spectrum (b) of the APMG with 20 stator core modules, cogging torque profile (c) and harmonic spectrum (d) of the APMG with 60 stator core modules.

in an electrical period, respectively:

$$\frac{\mathrm{LCM}(2p, m)}{p} i = \frac{\mathrm{LCM}(100, 20)}{50} i = 2i, \quad i \epsilon \mathbb{N}, \tag{19}$$

$$\frac{\mathrm{LCM}(2p, m)}{p} i = \frac{\mathrm{LCM}(100, 60)}{50} i = 6i, \quad i \epsilon \mathbb{N}. \tag{20}$$

Instead, according to (2), the following harmonic orders of the NHCs are expected in an electrical period:

$$\frac{\mathrm{LCM}(2p, N_s)}{p} i = \frac{\mathrm{LCM}(100, 120)}{50} i = 12i, \quad i \epsilon \mathbb{N}. \tag{21}$$

Fig. 4 shows the cogging torque waveforms and harmonic spectra of the two AMPG topologies obtained by means of a TWM FEA ($N_{pos} = 150$), which requires about 90 minutes to be performed. Note that the orders of the AHCs agree with (19) and (20). Moreover, the amplitude of the NHCs is negligible if compared with the amplitude of the AHCs. The peak-to-peak values of the cogging torque are 16.68 Nm and 1.39 Nm, respectively. The dominant harmonic components of the APMGs with 20 and 60 stator core modules are respectively the 2nd and the 6th ones; moreover, most of the cogging torque of these machines can be reduced by suppressing these harmonic components. Therefore, only one sinusoidal profile is introduced to suppress the 2nd harmonic component of APMG with 20 stator core modules. According to the design formula (8), the spatial frequency of this profile must be $100/2\pi\,\mathrm{rad}^{-1}$. Instead, to suppress the 6th harmonic component of the APMG with 60 modules, a sinusoidal profile with a spatial frequency of $300/2\pi\,\mathrm{rad}^{-1}$ is adopted.

To determine the amplitudes and phase shifts of the introduced sinusoidal profiles, the approach described in Subsection III-C is employed. TABLE 3 and TABLE 4 report the results of five optimizations performed on the APMG with 20 stator core modules with $N_{DOE} = 100$ and $N_{DOE} = 250$, respectively. These tables report the optimized surrogate model topology, the mean squared error (MSE) on the test data, the solution $\boldsymbol{x}$ of the GA and the corresponding objective function evaluation $f_{\mathrm{NN}}(\boldsymbol{x})$, and the result of the FEA validation, $f_{FEA}(\boldsymbol{x})$, for each one of the five optimizations. Each sample has been obtained by using a TWM FEA with $N_{pos} = 24$. Note that, to better evaluate the performance of the proposed method, each of the five optimizations is performed by repeating the whole procedure described in Subsection III-C. An average reduction of the peak-to-peak cogging torque of 92.5% and 97.6% is obtained in the two cases, respectively. The accuracy of the surrogate models increases with the number of samples: in particular, the mean absolute percentage error (MAPE) between the surrogate objective function evaluation $f_{\mathrm{NN}}(\boldsymbol{x})$ and the TWM FEA $f_{\mathrm{FEA}}(\boldsymbol{x})$, is equal to 73.4% and 7.4% in the two cases, respectively. It can be also noticed that the optimization of the ANNs topology converges to similar solutions in the two cases. This result highlights how the ANNs accuracy depends on the topology adopted and confirms the importance of optimizing the ANNs topology.

TABLE 5 and TABLE 6 summarize the results on the APMG with 60 stator core modules with $N_{DOE} = 100$ and $N_{DOE} = 250$, respectively. Each sample has been obtained by using a TWM FEA with $N_{pos} = 36$. Also in this case, a significant average reduction of the peak-to-peak cogging torque (by 83.5% and 89.2% in the two cases) is achieved. The MAPE between $f_{\mathrm{NN}}(\boldsymbol{x})$ and $f_{\mathrm{FEA}}(\boldsymbol{x})$ is equal to 20.8% and 11.1% in the two cases, respectively. Considerations about the accuracy and topology optimization of the surrogate models made for the APMG with 20 stator core modules can be extended to the 60 modules machine. Fig. 5 shows the evolution of the best individuals among the GA generations obtained for the best designs of the APMG with 20 and 60 stator core modules, i.e. the ones obtained considering the parameters reported in the second row of TABLE 4 and TABLE 6, respectively. In both cases, the GA met the stop criterion before reaching the maximum number of generations. Approximately 4×10^4 evaluations of the objective function $f_{\mathrm{NN}}(\boldsymbol{x})$ with the ANNs have been performed during the GA optimization. The optimized shapes of the tooth tips of these two designs are shown in Fig. 6 and Fig. 7. It can be demonstrated that considering a profile with a

TABLE 3. Optimization results for the APMG with 20 stator core modules with $N_{DOE} = 100$.

	N_{HL} x N_{HN}	MSE [Nm^2]	x	$f_{NN}(x)$ [Nm]	$f_{FEA}(x)$ [Nm]
1	2x8	0.038	[0.307 0]	4.18	1.30
2	2x8	7.1x10^{-3}	[0.315 0.057]	0.67	1.13
3	3x6	0.104	[0.281 0]	3.15	2.41
4	2x8	0.044	[0.327 6.283]	0.47	0.43
5	2x10	0.060	[0.328 6.231]	0.34	0.97

TABLE 4. Optimization results for the APMG with 20 stator core modules with $N_{DOE} = 250$.

	N_{HL} x N_{HN}	MSE [Nm^2]	x	$f_{NN}(x)$ [Nm]	$f_{FEA}(x)$ [Nm]
1	2x10	4.8x10^{-4}	[0.327 6.283]	0.39	0.43
2	2x8	5.0x10^{-3}	[0.328 6.283]	0.41	0.40
3	2x10	7.6x10^{-4}	[0.328 6.283]	0.45	0.40
4	2x10	9.5x10^{-4}	[0.328 0.006]	0.38	0.40
5	3x8	1.4x10^{-3}	[0.328 0.002]	0.37	0.40

TABLE 5. Optimization results for the APMG with 60 stator core modules with $N_{DOE} = 100$.

	N_{HL} x N_{HN}	MSE [Nm^2]	x	$f_{NN}(x)$ [Nm]	$f_{FEA}(x)$ [Nm]
1	2x4	0.02	[0.055 6.129]	0.13	0.50
2	2x3	4x10^{-3}	[0.039 0.168]	0.18	0.17
3	2x5	0.01	[0.041 0.074]	0.20	0.19
4	2x5	4x10^{-3}	[0.042 0.001]	0.13	0.16
5	2x5	7x10^{-3}	[0.043 0.031]	0.14	0.14

TABLE 6. Optimization Results for the APMG with 60 stator core modules with $N_{DOE} = 250$.

	N_{HL} x N_{HN}	MSE [Nm^2]	x	$f_{NN}(x)$ [Nm]	$f_{FEA}(x)$ [Nm]
1	3x5	1.5x10^{-4}	[0.045 6.268]	0.15	0.21
2	3x5	1.3x10^{-4}	[0.043 0.048]	0.14	0.14
3	3x4	1.7x10^{-4}	[0.043 0.014]	0.14	0.16
4	2x5	1.4x10^{-4}	[0.043 0.027]	0.16	0.14
5	2x5	2.5x10^{-4}	[0.043 0.045]	0.14	0.14

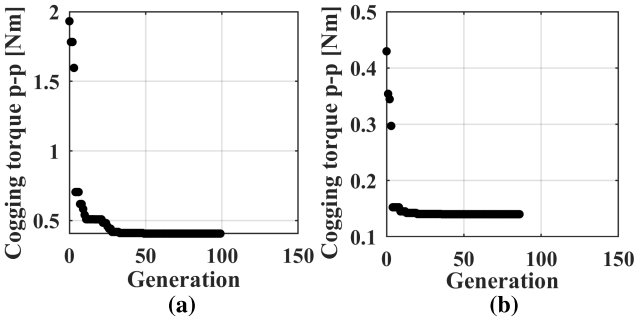

FIGURE 5. GA evolution of the best individuals: APMG with 20 stator core modules (a), APMG with 60 stator core modules (b).

spatial frequency equal to $100/2\pi\,\mathrm{rad}^{-1}$, 6 different shapes are obtained. Instead, when the spatial frequency is equal to $300/2\pi\,\mathrm{rad}^{-1}$, only two different shapes are obtained.

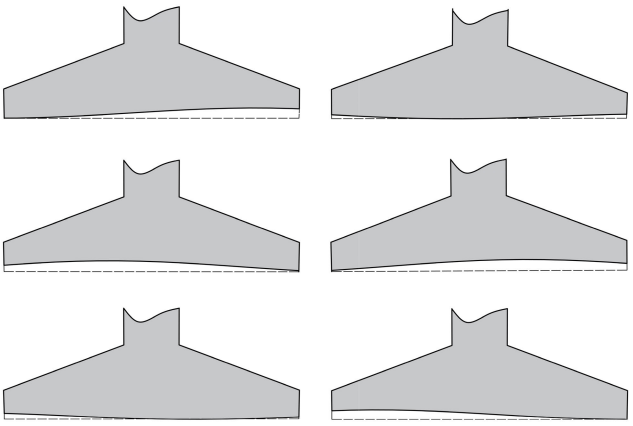

FIGURE 6. Optimized shapes of the tooth tips of the APMG with 20 stator core modules.

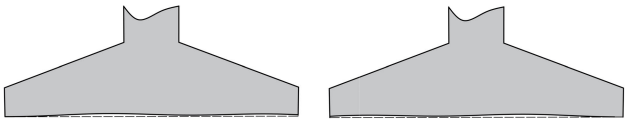

FIGURE 7. Optimized shapes of the tooth tips of the APMG with 60 stator core modules.

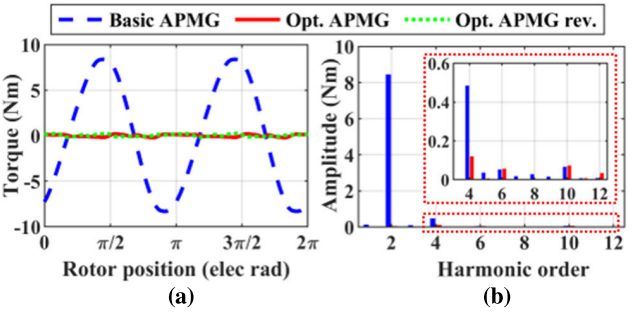

FIGURE 8. Cogging torque profile (a) and harmonic spectrum (b) of the optimized APMG with 20 stator core modules.

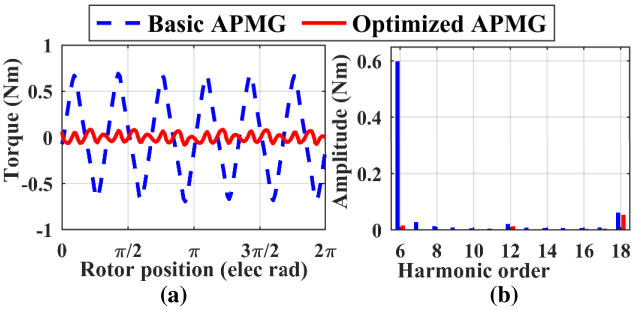

FIGURE 9. Cogging torque profile (a) and harmonic spectrum (b) of the optimized APMG with 60 stator core modules.

Fig. 8 and Fig. 9 show the waveforms and the harmonic spectra of the cogging torque for the two optimized designs. Both waveforms have been obtained by means of a TWM FEA with $N_{pos} = 150$. Compared to the base machine, the dominant cogging torque harmonic components have been drastically suppressed, whereas the other harmonics have not been substantially affected by the introduced sinusoidal

TABLE 7. Computational times.

Steps/operations	Time [s]
FEA, $N_{pos} = 24$ (1 instance)	720
FEA, $N_{pos} = 36$ (1 instance)	1320
ANN topology optimization	3600
ANN output computation (1000 instances)	10.5

profiles. This is particularly noticeable comparing the 12th and 18th harmonic components of the basic and optimized designs of the APMG with 60 stator core modules in Fig. 9(b). Fig. 8 also reports the cogging torque profile at reverse rotation direction, demonstrating how the cogging torque is not affected by the rotation direction, according to the theoretical study. Finally, TABLE 7 reports the computational times of the main steps of the proposed optimization procedure performed on an Intel Xeon CPU E5-1620 v3 @ 3.50 GHz. The computational effort required by the ANN to calculate the cogging torque corresponding to a given solution $\boldsymbol{x}$ is very limited: this means that most of the time spent by the proposed optimization procedure is required by the evaluation of the DoE.

B. RESULTS WITHOUT USING THE DESIGN FORMULA

To further validate the theoretical study presented in Subsection III-A, this subsection provides the results achieved by introducing sinusoidal profiles with spatial frequencies which do not respect (8). In particular, Fig. 10 shows the results of a TWM FEA ($N_{pos} = 150$) performed on the three different designs of the APMG with 20 stator core modules with the following sinusoidal profiles:

- First case: spatial frequency, amplitude and phase $f_{IHC_1} = 150/2\pi\,\text{rad}^{-1}$, $A_1 = 0.3$ mm and $\varphi_1 = 0$.
- Second case: spatial frequency, amplitude and phase $f_{IHC_1} = 200/2\pi\,\text{rad}^{-1}$, $A_1 = 0.3$ mm and $\varphi_1 = 0$.
- Third case: spatial frequency, amplitude and phase $f_{IHC_1} = 150/2\pi\,\text{rad}^{-1}$, $A_1 = 0.3$ mm and $\varphi_1 = 0$ and $f_{IHC_2} = 200/2\pi\,\text{rad}^{-1}$, $A_2 = 0.3$ mm and $\varphi_2 = 0$.

In the first case, the introduced sinusoidal profile does not affect the cogging torque as predicted by the theoretical study, i.e., since the harmonics of F_m^2 have a spatial frequency which is an integer multiple of $100/2\pi\,\text{rad}^{-1}$, no harmonics of F_m^2 are isofrequential with the airgap permeance function harmonic related to the introduced sinusoidal profile; thus, according to (5), the contribution to the cogging torque is none. Compared to the basic design, the amplitude of the harmonics is slightly reduced due to the average length increase of the airgap caused by the introduction of the sinusoidal profile.

In the second case, as expected, the introduced sinusoidal profile affects only the 4th harmonic component. In particular, compared to the basic design, the amplitude of the 4th harmonic component is increased since the amplitude and phase shift of the introduced sinusoidal profile have not been optimized to reduce the cogging torque.

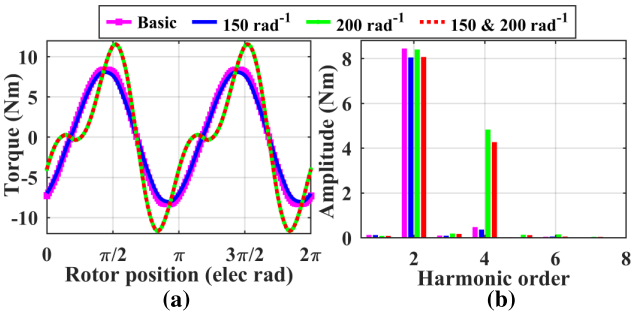

FIGURE 10. Cogging torque profile (a) and harmonic spectrum (b) of the APMG shaped with different sinusoidal profiles.

Note that, in the last case, the resulting torque is similar to the torque of the APMG with the sinusoidal profile with a spatial frequency of $200/2\pi\,\text{rad}^{-1}$. The amplitudes of the harmonics are slightly reduced since the average airgap length is greater than in the previous case. This result confirms the proposed theoretical study and the validity of the superposition principle adopted to study the effect of the airgap permeance function harmonics on the cogging torque.

C. COMPARISON WITH OTHER METHODS

In this subsection, a comparison with two other existing methods is presented. The first method is the topological optimization (TO) of the tooth tips proposed in [27], while the second approach is based on the slot openings shifting proposed in [4]. Both methods have been implemented on the APMG with 60 modules. In particular, according to the design formula (20) of [27], two different shapes of the tooth tips must be independently optimized by means of the topological optimization for the considered machine. Similarly, according to [4], in order to shift the slot openings, two different widths of the tooth tips are employed.

The topological optimization has been performed considering the same approach based on surrogate models described in Section III-C and the tooth tips have been discretized with 7 elements, called subteeth, as shown in Fig. 11. The vector of the design variables includes a binary quantity (0:air 1:iron) for each subteeth of the two tooth tip shapes plus a final variable representing the depth of the subteeth. The results obtained with $N_{DOE} = 250$ and $N_{DOE} = 400$ are shown in TABLE 8 and TABLE 9, respectively. An average reduction of the peak-to-peak cogging torque by 58.1% and 50.1% is obtained, while the MAE between $f_{\text{NN}}(\boldsymbol{x})$ and $f_{\text{FEA}}(\boldsymbol{x})$ is equal to 73.3% Nm and 78.4%, respectively. Note that, also in this case the optimization of the ANNs topology converges to similar solutions, but the accuracy of the surrogate models is lower compared to the ones obtained with the harmonic shaping of the tooth tips. This is the reason why the performances of the TO are lower if compared with the proposed method, even assigning a remarkable advantage to the former, i.e., a higher quantity of samples available to train the surrogate models. The high number of design variables required by the TO makes the prediction of the cogging torque more difficult. Therefore, compared to the method proposed in this paper, the

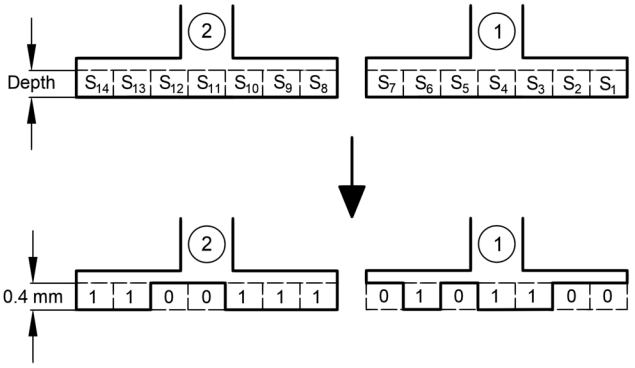

FIGURE 11. Example of two independent tooth tips discretized with a layer of 7 subteeth: $x =$ [0 0 1 1 0 1 0 11 1 0 0 1 1 0.4 mm].

TABLE 8. To results for the APMG with 60 stator core modules with $N_{DOE} = 250$ and 7 subteeth.

	N_{HL} X N_{HN}	MSE [Nm^2]	$\boldsymbol{x}$	$f_{\text{NN}}(\boldsymbol{x})$ [Nm]	$f_{\text{FEA}}(\boldsymbol{x})$ [Nm]
1	1x4	0.2174	1 1 1 0 1 0 0 0 1 1 1 0 0 0 0 0.1753 mm	0.13	0.37
2	2x4	0.1768	1 0 0 1 0 1 0 1 1 0 0 0 0 1 0.1956 mm	0.13	0.40
3	1x6	0.2055	1 0 0 0 1 1 0 1 1 1 0 0 1 0 0.2289 mm	0.13	0.66
4	2x4	0.2291	1 0 1 1 1 0 0 0 0 1 1 0 0 0 0.0431 mm	0.14	1.04
5	2x4	0.2285	1 1 1 1 1 1 0 0 0 1 0 1 1 1 0.1528 mm	0.13	0.40

TABLE 9. To results for the APMG with 60 stator core modules with $N_{DOE} = 400$ and 7 subteeth.

	N_{HL} X N_{HN}	MSE [Nm^2]	$\boldsymbol{x}$	$f_{\text{NN}}(\boldsymbol{x})$ [Nm]	$f_{\text{FEA}}(\boldsymbol{x})$ [Nm]
1	1x6	0.1879	1 0 1 0 0 1 0 0 1 1 0 0 0 1 0.0972 mm	0.13	0.69
2	1x6	0.1730	1 1 0 1 1 0 0 0 0 0 0 1 0 1 0.1341 mm	0.13	0.38
3	1x6	0.1654	1 0 0 0 1 0 0 0 0 1 1 1 0 0 0 0.1998 mm	0.13	0.48
4	1x4	0.1568	1 1 0 0 1 1 1 0 1 0 1 0 1 1 0.0477 mm	0.13	1.02
5	2x4	0.1807	1 1 1 1 1 0 0 0 1 1 1 0 1 1 0.0504 mm	0.13	0.85

TO requires more sophisticated approaches to suppress the cogging torque of modular machines [27]. The TO has also been performed with 5 and 9 subteeth with $N_{DOE} = 400$. An average reduction of the peak-to-peak cogging torque of 72.0% and 49.9% has been achieved, with a MAPE between $f_{\text{NN}}(\boldsymbol{x})$ and $f_{\text{FEA}}(\boldsymbol{x})$ equal to 59.8% and 78.2%, respectively. Note that the improvement of the performances obtained with 5 subteeth further highlights the relationship bewteen the accuracy of the surrogate models and the number of the design variables.

The slot opening shifting is based on a unique design variable, i.e. the shift angle γ, as shown in Fig. 12. Due to the simplicity of the problem, the method can be investigated by evaluating a set of solutions obtained by the uniform sampling

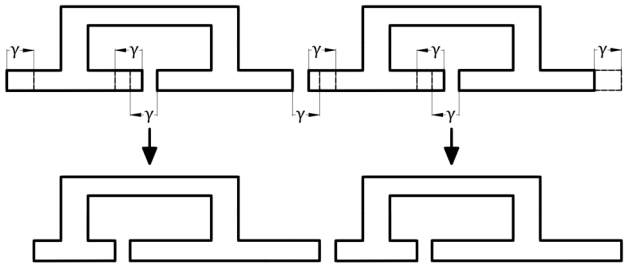

FIGURE 12. Stator core modules with slot openings shifted by γ.

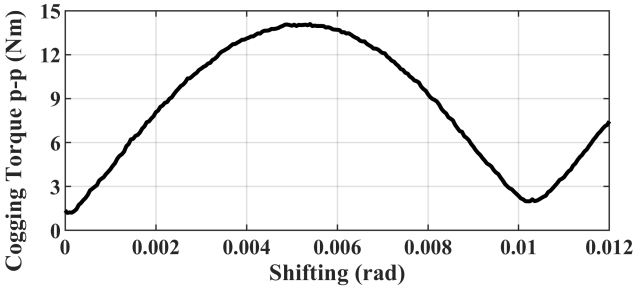

FIGURE 13. Peak-to-peak cogging torque values of the APMG with 60 stator core modules obtained with the slot openings shifting.

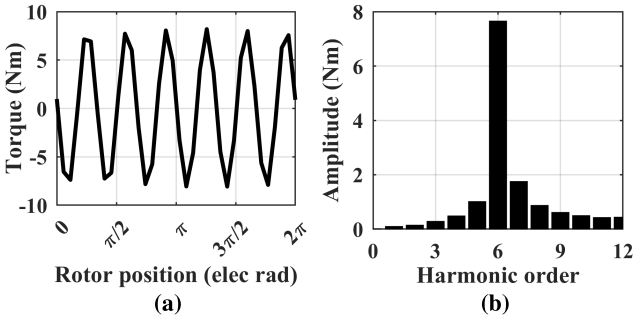

FIGURE 14. Cogging torque profile (a) and harmonic spectrum (b) of the APMG designed with the slot opening shifting method, with $\gamma = 0.0052$ rad.

of γ in its permissible range [0 γ_{lim}], where 0 corresponds to the basic slot openings position and γ_{lim} is the position corresponding to the minimum width of the stator tooth tip (i.e. the width of the stator teeth). Fig. 13 shows the results of 240 solutions in this interval obtained directly using the FEA with $N_{pos} = 36$, while Fig. 14 shows the cogging torque profile and harmonic spectrum with $\gamma = 0.0052$rad. As expected, the method affects the 6$^{\text{th}}$ harmonic component of the cogging torque. However, only few solutions slightly reduce the cogging torque of the considered machine. In fact, the lowest value of the peak-to-peak cogging torque obtained is 1.20 Nm, with a reduction of 12.4% with respect to the basic machine. This can be explained by considering that the cogging torque harmonic introduced by the slot opening shifting method may not match the amplitude of the 6$^{\text{th}}$ AHC. Indeed, since the width of the slot openings is fixed, the amplitude of the introduced harmonic component cannot be regulated to suppress the AHC. Instead, with the harmonic shaping and the TO methods, the amplitude of the introduced

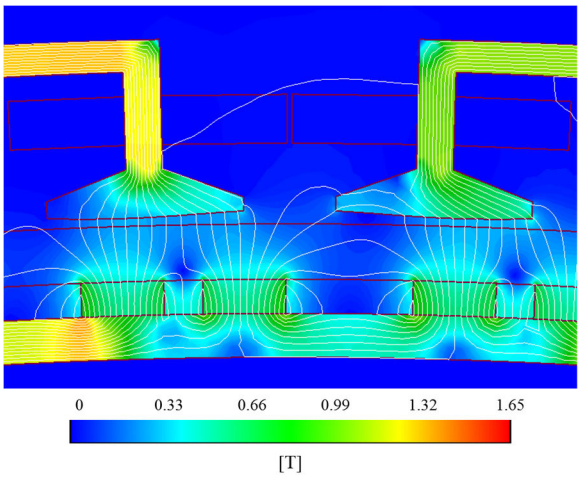

FIGURE 15. Flux density distribution at rated current of the optimized design of the APMG with 20 stator core modules.

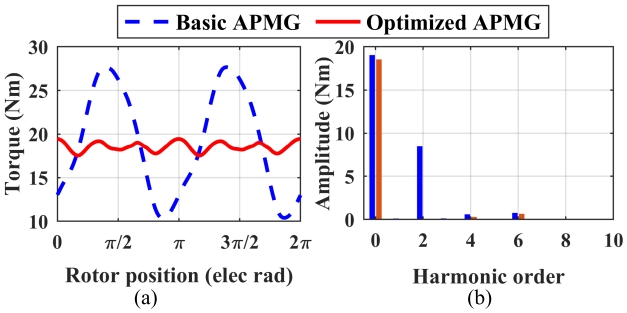

FIGURE 16. Torque profile (a) and harmonic spectrum (b) of the basic and optimized designs of the APMG with 20 stator core modules at rated current.

harmonic components can be adjusted to compensate the undesired AHCs.

D. ANALYSIS AT RATED CURRENT

This subsection reports the analysis of the basic and optimized designs of the APMG with 20 stator core modules at rated current, with the phase angle selected in agreement with the maximum torque per Ampere strategy. A sketch of the optimal machine with the modified shape of the tooth tips together with the flux density distribution under rated conditions is reported in Fig. 15. Fig. 16 shows the torque profiles and harmonic spectra of the two machines, highlighting how the 2nd harmonic component of the torque of the basic design has been perfectly suppressed at the expense of a slight reduction of the average torque (2.6%). Therefore, the impact of the proposed method on the rated torque is negligible. Also, the phase flux linkages before and after the optimization (Fig. 17) do not present appreciable differences. In fact, the average THD of the phases flux linkage is 2.24% for the basic design and 1.90% for the optimized design. Moreover, the average amplitudes are 0.166 Wb and 0.161 Wb for the basic and optimized design.

Table 10 reports a comparison of the loss components of the two machines at rated speed and current. The optimized

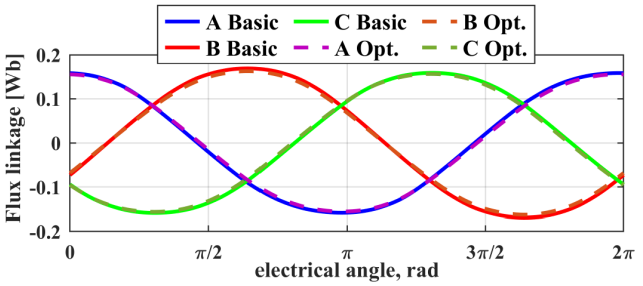

FIGURE 17. Phases flux linkage of the basic and optimized designs of the APMG with 20 stator core modules at rated current.

TABLE 10. Losses of the basic and optimized designs.

Losses components	Basic design [W]	Optimized design [W]
Copper losses	91.42	91.42
PM losses	7.19	5.64
Iron losses	35.02	33.30

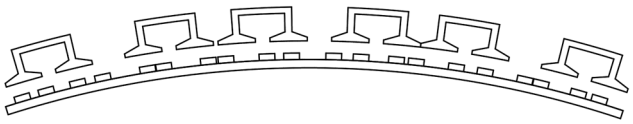

FIGURE 18. APMG with stator core modules and rotor magnets positioning tolerances according to the non-UUM.

design exhibits a slight reduction of the PM and iron losses and the impact on the overall efficiency is negligible. This analysis clearly proves that the proposed method ensures a significant improvement of the torque ripple of the APMG with negligible effects on other performance indexes of the machine.

E. ANALYSIS CONSIDERING MANUFACTURING AND ASSEMBLING TOLERANCES

This subsection analyzes the performance of the proposed method considering assembling and manufacturing tolerances of the modular PMM in the finite element model. The parameters affected by tolerances are the positions of magnets and stator modules, the shape of the tooth tips and the phase shift of the introduced sinusoidal profiles, as shown in Fig. 18 and Fig. 19. In these figures the manufacturing and assembling errors are accentuated to be more perceptible. Note that these errors affect both AHCs and IHCs of the cogging torque and may potentially compromise the effectiveness of the optimization. It is also worth noticing that manufacturing and assembling tolerances are sources of other AHCs of the cogging torque, as illustrated in [39] and [40].

According to typical manufacturing techniques, the considered positioning and phase shift tolerances are ±0.05° [39]. Instead, regarding the tooth tips shape, typical tolerances of the wire Electric Discharge Machining (EDM) technique are considered, i.e., ±0.0063 mm. To analyze the impact of the assembling and manufacturing tolerances,

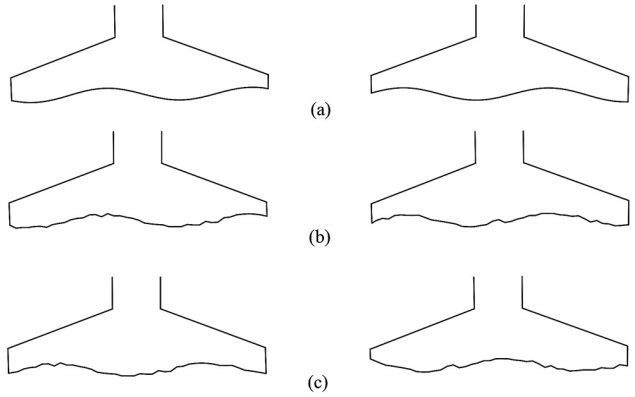

FIGURE 19. Manufacturing tolerances of the tooth tips shapes with the non-UUM: (a) reference design, (b) design with shape tolerances, (c) design with shape and phase shift tolerances.

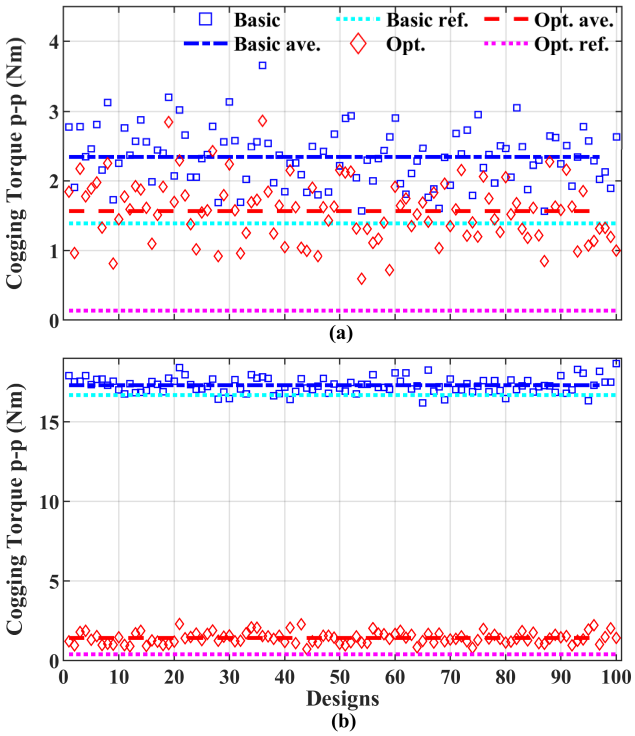

FIGURE 20. Performance analysis considering assembling and manufacturing tolerances with the non-UUM: (a) APMG with 60 stator core modules, (b) APMG with 20 stator core modules.

the reference basic and optimized models of the APMG with 20 and 60 modules have been modified by introducing parameter errors using the non-uniform uncertainties method (non-UUM). According to the non-UUM, each magnet and stator module of the APMG has its own position error, while each point of the sinusoidal shape of the tooth tips has its own amplitude error. The errors are generated assuming a normal distribution with zero-mean and standard deviation $\sigma = (USL - LSL)/6$, where USL and LSL are the upper and lower boundaries of the tolerance range, respectively [39]. Fig. 20 reports the analysis of the basic and optimized APMG with 60 and 20 stator core modules. The average

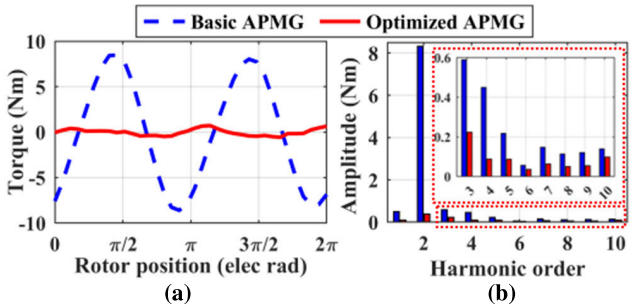

FIGURE 21. Cogging torque profile (a) and harmonic spectrum (b) of the optimized APMG with 20 stator core modules with assembling and manufacturing tolerances.

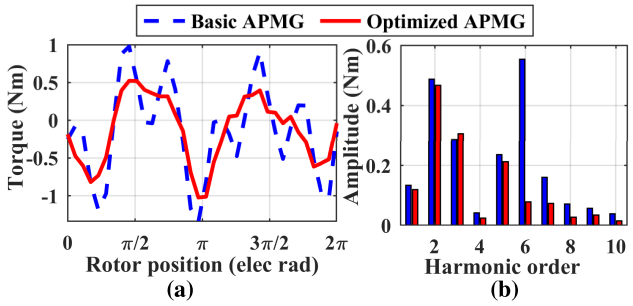

FIGURE 22. Cogging torque profile (a) and harmonic spectrum (b) of the optimized APMG with 60 stator core modules with assembling and manufacturing tolerances.

peak-to-peak cogging torque values of the basic APMGs considering the assembling and manufacturing tolerances are 2.34 Nm and 17.32 Nm. Therefore, the cogging torque of the non-optimized APMGs on average is increased by 0.98 Nm and 0.65 Nm, respectively (gaps between blue and cyan lines). Instead, the average peak-to-peak cogging torque values of the optimized APMGs considering the assembling and manufacturing tolerances are 1.56 Nm and 1.42 Nm, with a reduction of 0.78 Nm and 15.90 Nm compared to the average cogging torque of the basic machines with manufacturing and assembling uncertainties (gaps between blue and red lines). The difference between the cogging torque of the reference basic and optimized designs of the two APMGs are instead 1.25 Nm and 16.28 Nm, respectively (gaps between cyan and magenta lines). By comparing the gaps between cyan and magenta lines with gaps between blue and red lines, the differences are 0.47 Nm and 0.38 Nm. Therefore, in both cases, the performances of the methods are marginally affected by the manufacturing and assembling tolerances. This is more evident when comparing the harmonic spectra of two designs of the basic and optimized APMGs affected by tolerances, as in Fig. 21 and Fig. 22. In particular, the designs no. 25 have been analyzed for both APMGs, which have peak-to-peak cogging torque value near the average values shown in Fig. 18. The dominant harmonic components of both APMGs (i.e. 2^{nd} and 6^{th} harmonic component for the APMGs with 20 and 60 modules, respectively) have been almost suppressed. However, the cogging torque is affected by other AHCs introduced by the tolerances.

V. CONCLUSION

In this paper, an effective design methodology to suppress the cogging torque of modular permanent magnet machines has been presented. Sinusoidal profiles have been used to shape the stator tooth tips of the machine. The quantity and the frequency of the sinusoidal profiles to be introduced have been determined through an analytical study. In particular, a simple design formula has been derived which allows a fast computation of the spatial frequency of the sinusoidal profiles. Moroever, the optimal amplitude and phase shift of the sinusoidal profiles have been determined by using ANN-based surrogate models and a GA.

The effectiveness of the proposed method has been investigated considering two PMMs with different number of stator core modules. In both cases, a reduction of the cogging torque higher than 80% has been obtained, with a perfect suppression of the dominant cogging torque harmonics. Also, the comparison with other existing methods further higlighted the strengths of the proposed approach. Finally, an additional analysis demonstrates the effectiveness of the proposed method against manufacturing and assembling tolerances.

REFERENCES

[1] N. J. Baker, D. J. B. Smith, M. C. Kulan, and S. Turvey, "Design and performance of a segmented stator permanent magnet alternator for aerospace," *IEEE Trans. Energy Convers.*, vol. 33, no. 1, pp. 40–48, Mar. 2018.

[2] G. J. Li, Z. Q. Zhu, W. Q. Chu, M. P. Foster, and D. A. Stone, "Influence of flux gaps on electromagnetic performance of novel modular PM machines," *IEEE Trans. Energy Convers.*, vol. 29, no. 3, pp. 716–726, Sep. 2014.

[3] G.-J. Li, X.-B. Liang, Z.-Q. Zhu, J. Ojeda, and M. Gabsi, "Vibrations and acoustic noise analyses of modular SPM machines," in *Proc. IEEE Energy Convers. Congr. Expo. (ECCE)*, Detroit, MI, USA, Oct. 2020, pp. 5567–5573.

[4] G. J. Li, B. Ren, Z. Q. Zhu, Y. X. Li, and J. Ma, "Cogging torque mitigation of modular permanent magnet machines," *IEEE Trans. Magn.*, vol. 52, no. 1, pp. 1–10, Jan. 2016.

[5] E. Fleurot, F. Sculiller, and J.-F. Charpentier, "Analytical models for fast and accurate calculation of electromagnetic performances of segmented permanent magnet synchronous machines with large angular gaps," *Appl. Sci.*, vol. 11, no. 1, p. 459, Jan. 2021.

[6] G. Dajaku and D. Gerling, "Low costs and high-efficiency electric machines," in *Proc. 2nd Int. EDPC*, Nuremberg, Germany, Oct. 2012, pp. 1–7.

[7] G. J. Li, Z. Q. Zhu, M. Foster, and D. Stone, "Comparative studies of modular and unequal tooth PM machines either with or without tooth tips," *IEEE Trans. Magn.*, vol. 50, no. 7, pp. 1–10, Jul. 2014.

[8] Y. Sui, Z. Yin, L. Cheng, P. Zheng, D. Tang, C. Chen, and C. Wang, "Multiphase modular fault-tolerant permanent-magnet machine with hybrid single/double-layer fractional-slot concentrated winding," *IEEE Trans. Magn.*, vol. 55, no. 9, pp. 1–6, Sep. 2019.

[9] F. Xu, Z. Q. Zhu, T. R. He, Y. Wang, H. Bin, D. Wu, L. M. Gong, and J. T. Chen, "Influence of stator gap on electromagnetic performance of 6-slot/2-pole modular high speed permanent magnet motor with toroidal windings," *IEEE Access*, vol. 9, pp. 94470–94494, 2021.

[10] G. J. Li, B. Ren, Z. Q. Zhu, M. P. Foster, and D. A. Stone, "Demagnetization withstand capability enhancement of surface mounted PM machines using stator modularity," *IEEE Trans. Ind. Appl.*, vol. 54, no. 2, pp. 1302–1311, Mar./Apr. 2018.

[11] J.-X. Shen, S. Cai, J. Yuan, S. Cao, and C.-W. Shi, "Cogging torque in SPM machine with segmented stator," *COMPEL, Int. J. Comput. Math. Elect. Electron. Eng.*, vol. 35, no. 2, pp. 641–654, 2016.

[12] J. Yuan, C. Shi, and J. Shen, "Analysis of cogging torque in surface-mounted permanent magnet machines with segmented stators," in *Proc. 17th Int. Conf. Electr. Mach. Sys. (ICEMS)*, Hangzhou, China, Oct. 2014, pp. 2513–2516.

[13] X. Ge, Z. Q. Zhu, G. Kemp, D. Moule, and C. Williams, "Optimal step-skew methods for cogging torque reduction accounting for three-dimensional effect of interior permanent magnet machines," *IEEE Trans. Energy Convers.*, vol. 32, no. 1, pp. 222–232, Mar. 2017.

[14] M. G. Angle, J. H. Lang, J. L. Kirtley, S. Kim, and D. Otten, "Cogging torque reduction in permanent-magnet synchronous machines with skew," in *Proc. 22nd Int. Conf. Electr. Mach.*, Lausanne, Switzerland, Sep. 2016, pp. 207–211.

[15] G. Zhao, W. Hua, X. Zhu, and G. Zhang, "The influence of dummy slots on stator surface-mounted permanent magnet machines," *IEEE Trans. Magn.*, vol. 53, no. 6, pp. 1–5, Jun. 2017.

[16] H. C. Yu, B. S. Yu, J. T. Yu, and C. K. Lin, "A dual notched design of radial-flux permanent magnet motors with low cogging torque and rare earth material," *IEEE Trans. Magn.*, vol. 50, no. 11, pp. 1–4, Nov. 2014.

[17] D. Wu and Z. Q. Zhu, "Design tradeoff between cogging torque and torque ripple in fractional slot surface-mounted permanent magnet machines," *IEEE Trans. Magn.*, vol. 51, no. 11, pp. 1–4, Nov. 2015.

[18] T. Liu, S. Huang, J. Gao, and K. Lu, "Cogging torque reduction by slot-opening shift for permanent magnet machines," *IEEE Trans. Magn.*, vol. 49, no. 7, pp. 4028–4031, Jul. 2013.

[19] S.-M. Hwang, J.-B. Eom, G.-B. Hwang, W.-B. Jeong, and Y.-H. Jung, "Cogging torque and acoustic noise reduction in permanent magnet motors by teeth pairing," *IEEE Trans. Magn.*, vol. 36, no. 5, pp. 3144–3146, Sep. 2000.

[20] A. R. Pramurti and O. Y. Hutajulu, "The design of radial flux permanent magnet generator on low speed wind turbine to reduce cogging torque," in *Proc. Electr. Power, Electron., Commun., Contr. Informat. Semin. (EECCIS)*, Batu, Indonesia, Oct. 2018, pp. 68–72.

[21] D. Žarko, D. Ban, and T. A. Lipo, "Analytical solution for cogging torque in surface permanent-magnet motors using conformal mapping," *IEEE Trans. Magn.*, vol. 44, no. 1, pp. 52–65, Jan. 2008.

[22] V. Z. Faradonbeh, S. T. Boroujeni, and N. Takorabet, "Optimum arrangement of PMs in surface-mounted PM machines: Cogging torque and flux density harmonics," *Electr. Eng.*, vol. 102, pp. 1117–1127, Feb. 2020.

[23] S. L. Ho, N. N. Chen, and W. N. Fu, "An optimal design method for the minimization of cogging torques of a permanent magnet motor using FEM and genetic algorithm," *IEEE Trans. Appl. Supercond.*, vol. 20, no. 3, pp. 861–864, Jun. 2010.

[24] Y. Park, J. Cho, and D. Kim, "Cogging torque reduction of single-phase brushless DC motor with a tapered air-gap using optimizing notch size and position," *IEEE Trans. Ind. Appl.*, vol. 51, no. 6, pp. 4455–4463, Jul. 2015.

[25] Z. Q. Zhu, Z. Azar, and G. Ombach, "Influence of additional air gaps between stator segments on cogging torque of permanent-magnet machines having modular stators," *IEEE Trans. Magn.*, vol. 48, no. 6, pp. 2049–2055, Jun. 2012.

[26] E. Brescia, M. Palmieri, G. L. Cascella, and F. Cupertino, "Optimal tooth tips design for cogging torque suppression of permanent magnet machines with a segmented stator core," in *Proc. Int. Conf. Electr. Mach. (ICEM)*, Gothenburg, Sweden, Aug. 2020, pp. 1930–1936.

[27] E. Brescia, D. Costantino, P. R. Massenio, V. G. Monopoli, F. Cupertino, and G. L. Cascella, "A design method for the cogging torque minimization of permanent magnet machines with a segmented stator core based on ANN surrogate models," *Energies*, vol. 14, no. 7, p. 1880, Mar. 2021.

[28] S. Ruangsinchaiwanich, Z. Q. Zhu, and D. Howe, "Influence of magnet shape on cogging torque and back-EMF waveform in permanent magnet machines," in *Proc. Int. Conf. Electr. Mach. Syst.*, Nanjing, China, Sep. 2005, pp. 284–289.

[29] H. Wenjuan, G. Zhang, W. Liu, H. Liu, and Y. Wang, "Methods for reducing cogging force in permanent magnet machines: A review," *Energies*, vol. 16, no. 1, p. 422, Dec. 2022.

[30] A. Floris, A. Serpi, A. Damiano, and I. Hahn, "Torque harmonics minimization of double-stage magnetic gear transmission system," in *Proc. Ann. Conf. IEEE Ind. Electron. Soc. (IECON)*, Lisbon, Portugal, Oct. 2019, pp. 2751–2757.

[31] D. Lee, S. Lee, J.-W. Kim, C.-G. Lee, and S.-Y. Jung, "Intelligent memetic algorithm using GA and guided MADS for the optimal design of interior PM synchronous machine," *IEEE Trans. Magn.*, vol. 47, no. 5, pp. 1230–1233, May 2011.

[32] S. Barmada, N. Fontana, L. Sani, D. Thomopulos, and M. Tucci, "Deep learning and reduced models for fast optimization in electromagnetics," *IEEE Trans. Magn.*, vol. 56, no. 3, pp. 1–4, Mar. 2020.

[33] M. H. Mohammadi, T. Rahman, R. Silva, M. Li, and D. A. Lowther, "A computationally efficient algorithm for rotor design optimization of synchronous reluctance machines," *IEEE Trans. Magn.*, vol. 52, no. 3, pp. 1–4, Mar. 2016.
[34] I. Pan, M. Babei, A. Korre, and S. Durucan, "Artificial neural network based surrogate modelling for multi—Objective optimisation of geological CO_2 storage operations," *Energy Proc.*, vol. 63, pp. 3483–3491, Dec. 2014.
[35] F. Arifin, H. Robbani, T. Annisa, and N. N. M. I. Ma'arof, "Variations in the number of layers and the number of neurons in artificial neural networks: Case study of pattern recognition," *J. Phys., Conf.*, vol. 1413, Nov. 2019, Art. no. 012016.
[36] J. Gao, L. Dai, and W. Zhang, "Improved genetic optimization algorithm with subdomain model for multi-objective optimal design of SPMSM," *CES Trans. Electr. Mach. Syst.*, vol. 2, no. 1, pp. 160–165, Mar. 2018.
[37] A. Panichella, R. Oliveto, M. D. Penta, and A. D. Lucia, "Improving multi-objective test case selection by injecting diversity in genetic algorithms," *IEEE Trans. Softw. Eng.*, vol. 41, no. 4, pp. 358–383, Apr. 2015.
[38] M. Palmieri, S. Bozzella, G. L. Cascella, M. Bronzini, M. Torresi, and F. Cupertino, "Wind micro-turbine networks for urban areas: Optimal design and power scalability of permanent magnet generators," *Energies*, vol. 11, no. 10, p. 2759, Oct. 2018.
[39] Y. Yang, N. Bianchi, C. Zhang, X. Zhu, H. Liu, and S. Zhang, "A method for evaluating the worst-case cogging torque under manufacturing uncertainties," *IEEE Trans. Energy Conv.*, vol. 35, no. 4, pp. 1837–1848, Dec. 2020.
[40] L. Gasparin, A. Cernigoj, and R. Fiser, "Additional cogging torque components due to asymmetry in stator back iron of PM synchronous motors," *COMPEL-Int. J. Comput. Math. Elect. Electron. Eng.*, vol. 30, no. 3, pp. 894–905, May 2011.

ELIA BRESCIA was born in Putignano, Bari, Italy. He received the B.S., M.S. (Hons.), and Ph.D. degrees in electrical engineering from the Polytechnic University of Bari, Bari, in 2015, 2018, and 2022, respectively. Since 2022, he has been a Research Assistant with the Laboratory of Electrical Machines and Drives, Polytechnic University of Bari. His research interests include design, control, and parameter identification of electrical machines.

MARCO PALMIERI (Member, IEEE) received the M.Sc. (Hons.) and Ph.D. degrees in electrical engineering from the Polytechnic University of Bari, Italy, in 2011 and 2016, respectively. From 2018 to 2022, he was a Research Fellow with the Polytechnic University of Bari. He was a Visiting Scholar with the University of Nottingham, U.K., in 2014, and Saarland University, in 2019. He is currently with the School of Engineering, Università degli Studi della Basilicata. His research interests include the modeling and analysis of electrical machines and the design of high-speed electrical machines by means of optimization algorithms and finite element analysis. He has co-received the Prize Paper Award from the IEEE Industrial Electronics Society Electrical Machines Committee, in 2015.

PAOLO R. MASSENIO received the M.Sc. (Hons.) and Ph.D. degrees in control engineering from the Polytechnic University of Bari, Italy, in 2017 and 2021, respectively. From 2019 to 2020, he was a Visiting Scholar with the University of Texas at Arlington, Arlington, TX, USA. He is currently a Research Fellow with the Polytechnic University of Bari. His research interests include the distributed control of microgrids, reinforcement learning for optimal control, novel control approaches for soft-robots, and system identification. He received the Best Paper Award from the IEEE Power Electronic Society, in 2021.

GIUSEPPE L. CASCELLA (Member, IEEE) received the M.Sc. (Hons.) and Ph.D. degrees in electrical engineering from the Polytechnic University of Bari, Italy, in 2001 and 2005, respectively. He is currently a Research Assistant with the Polytechnic University of Bari. He has published more than 70 peer-reviewed scientific articles on industry 4.0 and AI applications. He was a coordinator of more than 30 research and development industrial projects. He was the Founder (2015) and the CEO of Idea75.it. His research interests include design, control, and parameter identification and the cloud data analytics of electrical motors. He has won two EU Marie Curie Fellowships at the University of Nottingham, U.K., and the University of Malta. He is a member of the Italian National Order of Engineers. He received the 2018 AWS Activate Builder, "Cloud Data Analytics for Energy Efficiency," Amazon Web Services, in 2018; the Best Experiment in Open Call 2, BEinCPPS, H2020, EU funded project, in 2018; and the "SmartSupervisor for Cognitive Energy Efficiency," A&T Award for the Best Innovative i4.0 Solution, in 2017.

FRANCESCO CUPERTINO (Senior Member, IEEE) received the Laurea and Ph.D. degrees in electrical engineering from the Polytechnic University of Bari, Bari, Italy, in 1997 and 2001, respectively. Since 2001, he has been with the Department of Electrical and Information Engineering, Polytechnic University of Bari, where he is currently a Full Professor of converters, electrical machines, and drives. He is the Scientific Director of four public/private laboratories with the Polytechnic University of Bari, which enroll more than 50 researchers; the Laboratory Energy Factory Bari, with GE AVIO, aimed at developing research projects in the fields of aerospace and energy; the More Electric Transportation Laboratory, with CVIT SpA (BOSCH Group), aimed at developing technologies for sustainable mobility; Cyber Physical Systems AROL Bari, with AROL SpA, focused on closure systems for food and beverage; and Innovation for Mills, with Casillo Group and Idea75, focused in the Industry 4.0 applications for wheat processing. He has authored or coauthored more than 130 scientific articles in his research fields. His research interests include the design of synchronous electrical machines, the motion control of high-performance electrical machines, the applications of computational intelligence to control, and the sensorless control of ac electric drives. He was a recipient of two Best Paper Awards from the Electrical Machines Committee of the IEEE Industry Application Society and the Homonymous Committee of the IEEE Industrial Electronics Society, in 2015. He is currently the rector of the Politechnic University of Bari.

Open Access funding provided by 'Politecnico di Bari' within the CRUI CARE Agreement